Electronic structure, optical properties, and lattice dynamics of orthorhombic Cu$_2$CdGeS$_4$ and Cu$_2$CdSiS$_4$ semiconductors

Alexander P. Litvinchuk[*]

Texas Center for Superconductivity, University of Houston, Houston, Texas 77204-5002, USA

Volodymyr M. Dzhagan

Institute of Semiconductors Physics, National Academy of Sciences of Ukraine, Prospekt Nauky 45, 03028 Kyiv, Ukraine
and Semiconductor Physics, Technische Universität Chemnitz, D-09107 Chemnitz, Germany

Volodymyr O. Yukhymchuk, Mykhailo Ya. Valakh, and Ivan S. Babichuk

Institute of Semiconductors Physics, National Academy of Sciences of Ukraine, Prospekt Nauky 45, 03028 Kyiv, Ukraine

Oleg V. Parasyuk and Lyudmyla V. Piskach

Department of General and Inorganic Chemistry, Volyn National University, Voli Avenue 13, 43009 Lutsk, Ukraine

Ovidiu D. Gordan and Dietrich R. T. Zahn

Semiconductor Physics, Technische Universität Chemnitz, D-09107 Chemnitz, Germany

The dielectric function of orthorhombic Cu$_2$CdGeS$_4$ and Cu$_2$CdSiS$_4$ single crystals (space group $Pmn2_1$) is measured experimentally in the spectral range of 0.7–5.2 eV, and the results are interpreted via comparison with *ab initio* calculations. Polarized Raman-scattering measurements of both semiconductors are reported. All observed vibrational modes are assigned to specific lattice eigenmodes of the wurtz-stannite structure. Good agreement between theoretical and experimental mode frequencies is established. The differences in the experimental Raman spectra of the two compounds are well correlated with the effect of exchanging Si and Ge predicted by the theory. The strongest lines in the Raman-scattering spectra of both semiconductors are identified as being due to the "breathing" motion of GeS$_4$ and SiS$_4$ octahedra.

I. INTRODUCTION

Bulk materials, nanocrystals, and films of I$_2$-II-IV-VI$_4$ quaternary semiconducting compounds gained considerable attention in recent years [1–10]. This is stimulated by the fact that their properties are found to be appropriate for efficient applications in solar cells, nonlinear optical devices, thermoelectrics, photocatalysis, etc. [1–3,11–13]. However, a systematic understanding of the evolution of the electronic and structural properties with chemical composition and the type of cation sublattice ordering of these materials is still far from being achieved. Among quaternary compounds the majority of the research has been focused until now primarily on tin-based materials, particularly [5–7,14,15] Cu$_2$(Zn,Cd)Sn(S,Se)$_4$. Only some preliminary optical studies of Cu$_2$Zn(Si,Ge)(S,Se)$_4$ were recently reported [8,9,12,13,16]. As far as Cu$_2$CdGeS$_4$ and Cu$_2$CdSiS$_4$ semiconductors are concerned, their structural features were studied so far [17–21], whereas optical and electronic properties were only scarcely discussed in literature [20,22–24].

Recently the calculated electronic band structure of Cu$_2$CdGeS$_4$ of stannite and kesterite structural modifications was reported by Zhang *et al.* [11]. It was also recognized that, similar to ternary compounds, such as CuInS$_2$ [25,26], the so-called wurtzite-derived orthorhombic structures, such as wurtz stannite and wurtz kesterite are of principal importance as

they could be more energetically favorable than the "standard" tetragonal stannite and kesterite phases [6,13].

In this paper we present experimental spectroscopic ellipsometry data for Cu$_2$CdGeS$_4$ and Cu$_2$CdSiS$_4$ crystals of the wurtz-stannite structural modification (space group $Pmn2_1$, No. 31) which provide optical constants in the spectral range between 0.7 and 5.2 eV. These results are discussed in view of first-principles calculations of the electronic structure. Moreover, polarized Raman-scattering experiments were performed, which allowed the phonon modes to be identified according to their symmetry. All experimentally observed lines (41 and 42 for two compounds out of the expected 45) are assigned to the specific lattice eigenmodes via a comparison with results of *ab initio* lattice-dynamics calculations. We also discuss displacement patterns for the high-frequency modes of both materials and modes which exhibit the highest intensity in experimental Raman-scattering spectra.

II. SAMPLES, EXPERIMENTAL AND CALCULATION TECHNIQUES

Both Cu$_2$CdSiS$_4$ and Cu$_2$CdGeS$_4$ crystallize in the orthorhombic wurtz-stannite structure (space group $Pmn2_1$) with respective lattice parameters $a = 7.60$, $b = 6.48$, $c = 6.25$, $a = 7.70$, $b = 6.55$, and $c = 6.29$ Å [21,27]. All optical measurements were performed on natural surfaces of crystals, which were cleaned in an ultrasound bath in a mixture of ethanol and isopropanol to eliminate organic contamination

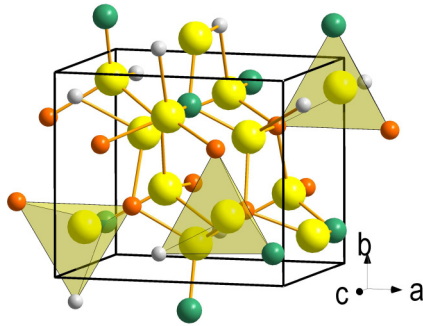FIG. 1. (Color online) Crystal structure of orthorhombic Cu_2CdGeS_4, featuring three crystallographically nonequivalent chalcogenide ions. Each tetrahedron around S is built of Ge, Cd, and two Cu's. S ions are shown in yellow, Ge ions are shown in green, Cd ions are shown in gray, and Cu ions are shown in orange.

on the surface. The samples studied were plateletlike or needlelike crystals with dimensions up to $10 \times 1 \times 0.5$ mm, grown by chemical vapor transport. The details of the sample preparation and their structural characterizations were reported previously [18,20]. The long axis of the platelets was shown to coincide with the crystallographic c axis, whereas the most developed facets were found to be (010) or $(0\bar{1}0)$. Both compounds exhibit p-type conductivity, and their transport properties might vary significantly depending on the growth conditions and postgrowth annealing [20].

As depicted in Fig. 1, half of the allowed tetrahedral voids of the hexagonal-close sulfur packing are occupied by two Cu atoms, the other half are occupied by one Cd and one Ge(Si) atom. The coordination of electronegative elements (sulfur) is also tetrahedral. This structure is described as the "normal tetrahedral" one (after Ref. [28]) and represents a limiting member of the wurtzite-derived Cu_2CdGeS_4 structure [27]. Our total energy calculations, which will be discussed below in more detail, show that the wurtz-stannite phase of Cu_2CdGeS_4 and Cu_2CdSiS_4 is energetically more favorable than the tetragonal stannite and kesterite structural modifications and the energy gain is equal to about 28 and 37 meV per atom, respectively.

A commercial J. A. Woollam Co., Inc. variable angle spectroscopic ellipsometer M-2000 T-Solar was used for measurements of the spectral dependence of the dielectric function [29] in the energy range between 0.7 and 5.2 eV with a step width of 0.02 eV. The measurements were performed from (010) facets of crystal so that the light reflection plane coincided with the (011) crystallographic plane. In this geometry both $\vec{E} \parallel c$ (p-polarized light) and $\vec{E} \perp c$ (s-polarized light) configurations were realizable. The facets of the crystals under investigation were large enough to accommodate a focused light beam with a diameter of about 0.5 mm. All measurements were performed at room temperature at incidence angles of $65°$, $70°$, and $75°$.

Raman-scattering and photoluminescence (PL) spectra were excited with the 647-nm line of a Kr^+ ion laser and the 514.5-nm line of an Ar^+ ion laser correspondingly and recorded with a Dilor XY triple spectrometer equipped with a Peltier cooled CCD detector. All measurements were performed in the backscattering configuration at a liquid-

nitrogen temperature using a Linkam stage (Raman scattering) and at room temperature (photoluminescence). The spectral resolution was about 2 cm^{-1}.

The first-principles calculations of the electronic ground state of $Cu_2CdGe(Si)S_4$ of wurtz-stannite structural modification were performed within the generalized gradient approximation [(GGA) and GGA + U] using the Perdew-Burke-Ernzerhof local functional [30] and the hybrid Becke three-parameter Lee-Yang-Parr functional [31] as implemented in the CASTEP code [32]. These approaches (out of many known, see Ref. [33] for a recent review) represent two widely used computational schemes to account for the on-site Cu(3d) electron correlations. Norm-conserving pseudopotentials were used. Prior to performing calculations the structure was relaxed while keeping lattice parameters fixed and equal to the experimentally determined ones so that forces on atoms in the equilibrium position did not exceed 2 meV/Å and the residual stress was below 0.01 GPa. A self-consistent field (SCF) tolerance better than 10^{-7} and a phonon SCF threshold of 10^{-12} were imposed. For calculations of the electronic structure and other relevant electronic properties an integration within the Brillouin zone was performed over an $8 \times 10 \times 10$ Monkhorst-Pack grid [34] in reciprocal space.

We have to mention that, despite the ground-state properties and the total energy of the system being the central quantity in the density functional theory (DFT), valuable information about the excited state can be obtained by evaluating the response to small perturbations [32]. In particular, a response to the electric field yields dielectric properties of the material, whereas a perturbation of atomic positions provides information on lattice vibrations. The electronic band-structure calculations of both Cu_2CdGeS_4 and Cu_2CdSiS_4 clearly show their semiconducting behavior. Fixed electron occupancy constraints were imposed on the self-consistent field energy minimization as a prerequisite for using the linear-response scheme [35] in the phonon calculations treating the atomic displacements as perturbations. Furthermore, an electric-field response along different crystallographic directions was estimated, which allows, in addition to the transverse-optical (TO) modes, a nonanalytical correction to longitudinal (LO) phonon frequencies at the Brillouin-zone center to be calculated. This is of principal importance for polar materials, such as $Cu_2CdGe(Si)S_4$ where the LO-TO splitting could be sufficiently large.

III. RESULTS AND DISCUSSION

A. Spectroscopic ellipsometry and electronic band structure

Here we will analyze spectroscopic ellipsometry data for $Cu_2CdGe(Si)S_4$ crystals, which are obtained for light polarized along the c axis ($\vec{E} \parallel c$) and perpendicular to it ($\vec{E} \perp c$). Comparison of the experimental data with those calculated within the first principles and the interpretation of the main spectral features are of primary interest. We begin with a brief analysis of the electronic band structure and the partial density of states.

Two different computational approaches were used to calculate the electronic band structure of Cu_2CdGeS_4 and Cu_2CdSiS_4. Within the GGA + U approximation (where U
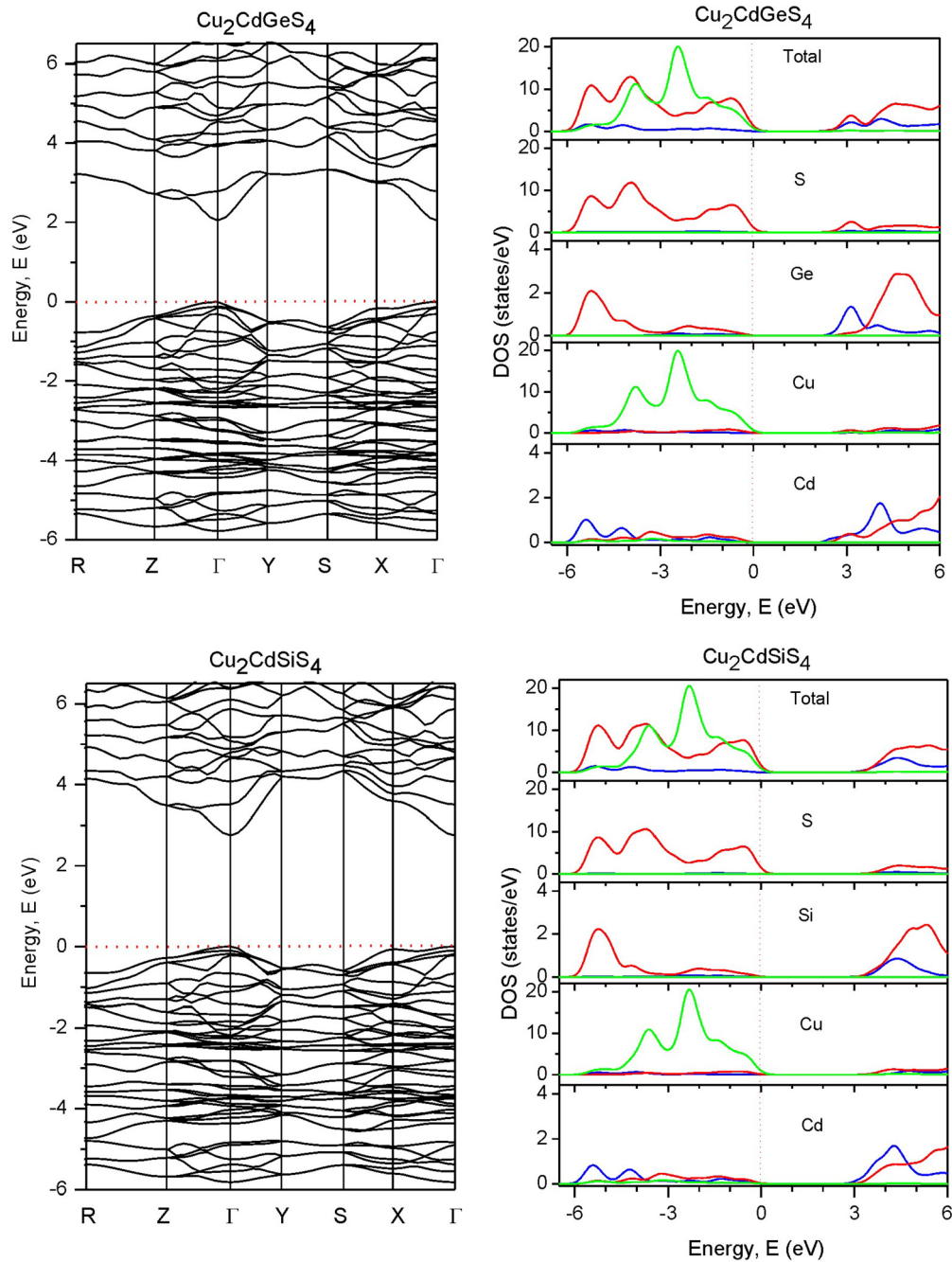
FIG. 2. (Color online) GGA $+U$ calculated electronic band structure (left column) and partial density of states (right column) of Cu_2CdGeS_4 and Cu_2CdSiS_4. Blue, red, and green lines correspond to contributions from s, p, and d states, respectively. The total density of states is shown in the top upper panel for each compound. Note an expanded vertical scale for Ge, Si, and Cd ions.

is the Hubbard parameter that takes into account the on-site repulsion for the $3d$-Cu states and was varied between 0 and 7.5 eV) the band-gap value E_g was found to vary between 0.97 and 1.65 eV upon increasing the U parameter. This approach, however, especially for $U \to 0$, is known to underestimate the magnitude of the band gap for insulating and semiconducting materials [36,37]. Increasing U values, apart from the evident "opening of the gap," is accompanied by the downshift in the intense Cu($3d$) peak in the density of states and a suppression of the $3d$-states contribution near the top of the valence band. On the other hand, it has only a minor effect on the conduction-

band structure and s and p states around the top of the valence band. This fact makes it plausible to apply a "scissor" operation (i.e., rigid shift of the conduction bands by certain amount) while comparing calculated results with experimental data [32,38]. Corresponding band structures as well as total and partial density of states for both compounds obtained in this matter are shown in Fig. 2 for $U = 2.5$ eV and scissor shifts 0.80 and 0.95 eV for Cu_2CdGeS_4 and Cu_2CdSiS_4, respectively.

The maximum of the valence bands and the minimum of the conduction bands occur at the Brillouin-zone center (Γ point) so that both materials are direct band-gap semiconductors.
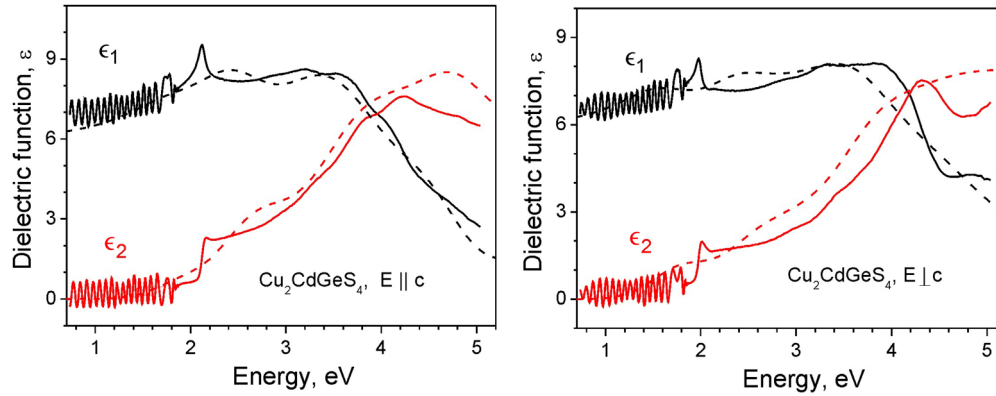
FIG. 3. (Color online) Polarized experimental (solid lines) and GGA + U calculated (dashed lines) spectral dependence of the real (ϵ_1 in black) and imaginary (ϵ_2 in red) parts of the dielectric function of Cu_2CdGeS_4 single crystals.

As the next step, we used the hybrid Becke functional, that takes into account some exact Hartree-Fock exchange and was shown to predict the band-gap energies of semiconductors with much higher accuracy [31,39]. In particular, this approach provided very reasonable data not only for binary III-V and II-VI semiconductors, but also for ternary chalcogenides of types $CuInS_2$, $CuAlS_2$, etc. [40]. Our calculations show that within this approach the band-gap values are $E_g = 2.31$ eV for Cu_2CdGeS_4 and $E_g = 2.86$ eV for Cu_2CdSiS_4, which, as we will see later, are slightly overestimated with respect to those obtained experimentally.

Apart from different magnitudes of the band gap and some differences in the distribution of the Cu(3d) bands in the valence zone, the remaining elements of the band structure in terms of band dispersion and their relative position seem to be very similar at first sight for two used computational approaches. However, a closer comparison with experimentally obtained ellipsometric data reveals that the GGA + U approach provides a better *quantitative* description of experimental spectral dependence of the dielectric function as depicted in Fig. 3. This is the main reason for using further the GGA + U calculations for the interpretation of experimental results.

Similar to other tetrahedrally coordinated chalcogenides [12,13] the top of the valence band of Cu_2CdGeS_4 is formed primarily by S(3p) and Cu(3d) bonding orbitals, whereas the bottom of the conduction band is formed by Ge(4s), S(4p), and Cd(5s) antibonding states. Thus, the magnitude of the band gap is mainly determined by the Ge-S hybridization. Our calculations show that the substitution of Zn for Cd, for example, does not influence either the magnitude of the band gap or the position and shape of the main electronic bands around the zone edges.

In the case of Cu_2CdSiS_4 the Cd-S hybridization becomes important. This fact follows from the calculated effect of Zn for Cd substitution, which does influence (widens) the band gap. One can also notice from Fig. 2 that Cd provides the largest s-states density at the bottom of the conduction band, which exceed the one for Si.

The experimentally determined spectral dependence of the dielectric function of Cu_2CdGeS_4 is shown in Fig. 3 by solid lines for light polarized along the c axis and perpendicular

to it. Pronounced interference fringes are observed in the low-frequency range of the spectra (transparency range of the material) due to the rather small sample thickness of about 100 μm and parallel surfaces of the crystalline platelet. At the same time, from the spectral dependence of the imaginary part of dielectric function ϵ_2 one can readily determine the position of the absorption onset, which directly defines the band-gap value and turns out to be 2.05 eV for $\overrightarrow{E} \parallel c$ and 1.93 eV for $\overrightarrow{E} \perp c$. As ϵ_1 and ϵ_2 are not independent but related via Kramers-Kronig transformation, it is not surprising to also observe respective peaks (gap features) in the ϵ_1 spectra for both polarizations [41]. Overall, a reasonable agreement on the quantitative level is observed between experimental and calculated spectral dependences of the dielectric function.

The positions of the observed features in ellipsometry are in close agreement with earlier reported optical transmission experiments, which yield the band-gap value of $E_g = 2.05$ eV [20] and about 1.85 eV [23]. Furthermore, our photoluminescence experiments, as shown in Fig. 4, which were performed under band-to-band excitation with $\lambda_{exc} = 514.5$ nm ($E_{exc} = 2.41$ eV), reveal a strong and relatively narrow (linewidth about 50 meV) peak with the maximum at 1.98 eV. Due to the close proximity of this luminescence peak to the band gap, it could be assigned to the band-to-band (excitonic) transition or to a transition involving shallow trap(s). The former origin is supported by the polarization behavior of the PL, which is strongly polarized and observed for light polarized perpendicular to the c axis of the crystal. A detailed temperature- and laser-power-dependent investigation in a broad spectral range is in progress, aiming at establishing the PL properties of Cu_2CdGeS_4 in detail.

Ellipsometric data for Cu_2CdSiS_4 (not shown here) reveal the band-gap features at about 2.78 eV. For this compound, however, the precise determination of the band gap was hindered by the presence of finite absorption below the band gap, which is apparently due to the presence of structural imperfections, such as disorder of the cation sublattice, point defects, etc. On the other hand, this disorder does not appear to be strong enough on a microscopic scale to affect vibrational spectra: The observed Raman-scattering lines, as we will see in the next section, do not exhibit any excessive linewidth broadening.
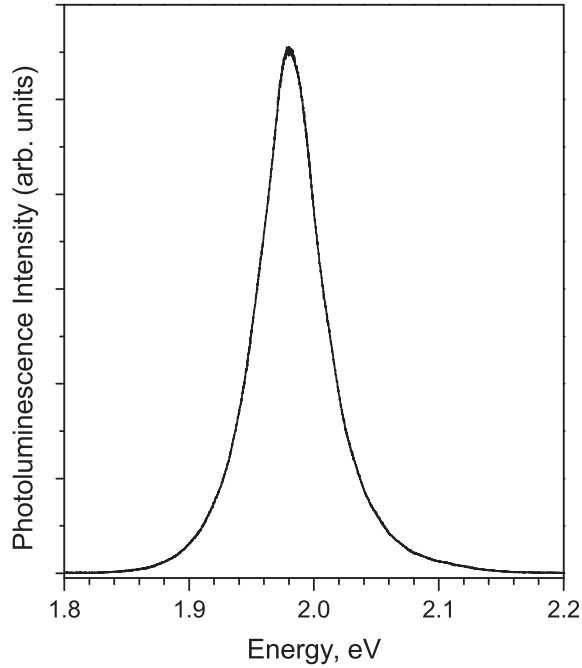
FIG. 4. Photoluminescence spectrum of Cu_2CdGeS_4 measured with $\lambda_{exc} = 514.5$ nm at room temperature.

B. Raman-scattering and lattice-dynamics calculations

Considering the lattice-dynamics properties of $Cu_2CdGe(Si)S_4$ in its wurtz-stannite structural modification (space group $Pmn2_1$) it is instructive to perform the group-theoretical analysis of the lattice phonon modes. The results of this analysis are summarized in Table I. First of all, we want to point out an increase in the number of modes that are allowed by symmetry in comparison with the stannite and kesterite structural polymorphs common for other quaternary chalcogenides, e.g., for extensively studied Cu_2ZnSnS_4 and $Cu_2ZnSnSe_4$ [7,42,43]. These two latter tetragonal compounds crystallize in body-centered lattices (space groups $I\bar{4}2m$ and $I\bar{4}$, respectively), and their primitive cell volume is only half with respect to the orthorhombic wurtz stannite so that there are 21 optical modes for these

TABLE I. Wyckoff position, site symmetry, and irreducible representations for nonequivalent atomic sites of the wurtz-stannite structure of $Cu_2CdGe(Si)S_4$ (space group $Pmn2_1$).

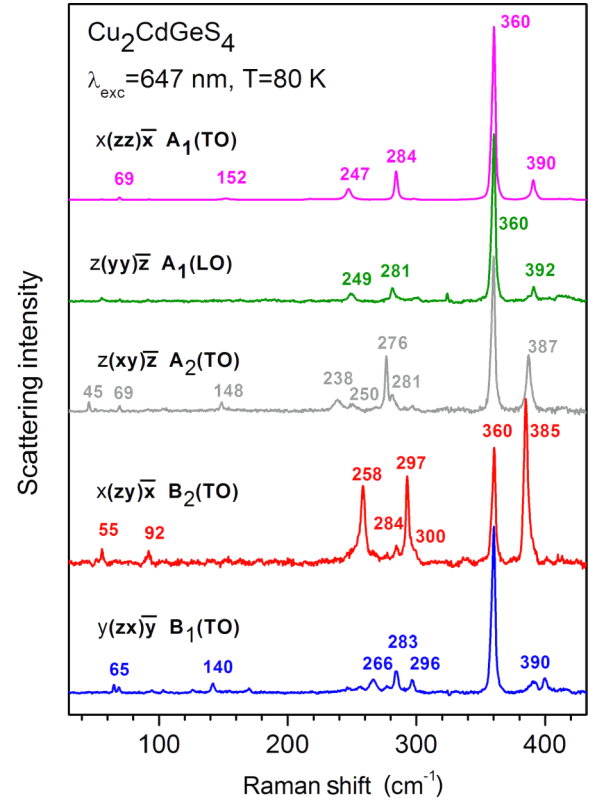| Atom	Wyckoff position	Site symmetry	Irreducible representations
Cu	4b	C_1	$3A_1 + 3A_2 + 3B_1 + 3B_2$
Zn	2a	C_s	$2A_1 + A_2 + B_1 + 2B_2$
Ge(Si)	2a	C_s	$2A_1 + A_2 + B_1 + 2B_2$
S(1)	2a	C_s	$2A_1 + A_2 + B_1 + 2B_2$
S(2)	2a	C_s	$2A_1 + A_2 + B_1 + 2B_2$
S(3)	4b	C_1	$3A_1 + 3A_2 + 3B_1 + 3B_2$
Mode classification			
$\Gamma_{acoustic} = A_1 + B_1 + B_2$			
$\Gamma_{Raman} = 13A_1 + 10A_2 + 9B_1 + 13B_2$			
$\Gamma_{IR} = 13A_1 + 9B_1 + 13B_2$			

FIG. 5. (Color online) Polarized Raman-scattering spectra of Cu_2CdGeS_4 measured at 80 K with an excitation wavelength of 647 nm. The corresponding scattering polarization and the mode symmetry are shown next to each spectrum.

structures. For the wurtz-stannite modification 45 optical vibrational modes are expected, all of which are Raman active due to the lack of inversion symmetry in the structure. A_1, B_1, and B_2 modes are simultaneously infrared active and thus might possess longitudinal-transverse (LO-TO) splitting due to a macroscopic electric field, generated by corresponding vibrations.

Here and further on we will use Porto notations for describing the Raman-scattering geometry: $a(bc)d$, where symbols outside the brackets (a and d) stand for the direction of the incident and scattered light, whereas symbols within the brackets (b and c) denote the polarization of the incident and scattered light, respectively. With this notation, the fully symmetric A_1 modes are expected to be active in (xx), (yy), and (zz) scattering configurations as it follows from the Raman-scattering selection rules [44]. A_2 modes are expected to appear in the (xy) and (yx) polarizations, B_1 modes are expected to appear in (xz) and (zx), and, finally, B_2 modes are expected to appear in (yz) and (zy). Polarized Raman-scattering spectra taken in several scattering geometries are shown in Figs. 5 and 6.

The most intensive line in the spectra of Cu_2CdGeS_4 is observed at 360 cm^{-1} and, as we will see later, appears to be a superposition of close-lying fully symmetric A_1 and B_2 lines. We noticed that some of the lines in the polarized Raman spectra are not strictly obeying the selection rules and could be observed with varying intensity in several scattering
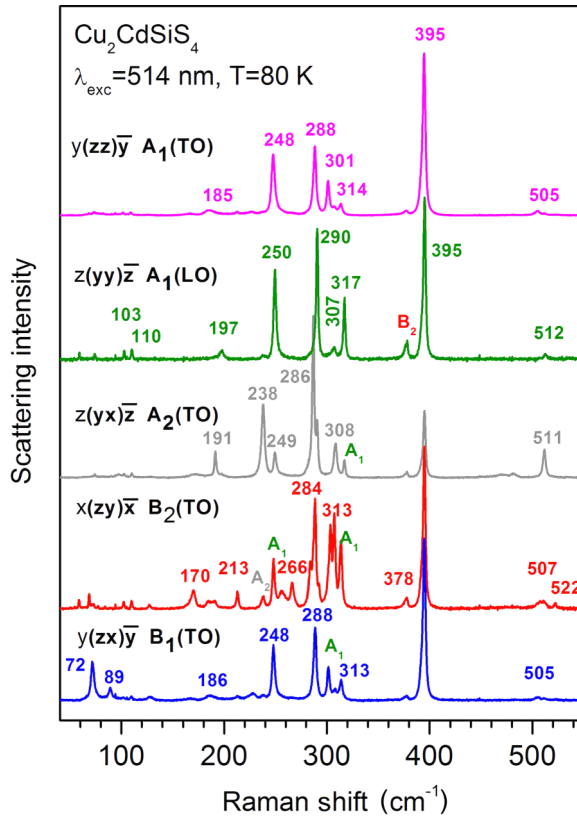
FIG. 6. (Color online) Polarized Raman-scattering spectra of Cu_2CdSiS_4 measured at 80 K with an excitation wavelength 514 nm. The corresponding scattering polarization and the mode symmetry are shown next to each each spectrum.

TABLE II. Experimental Raman- and DFT-calculated TO and LO lattice vibration frequencies of Cu_2CdGeS_4 (upper part) and Cu_2CdSiS_4 (lower part). The frequencies of the strongest experimental peaks are listed in bold and are marked in the experimental spectra shown in Figs. 5 and 6. All data are in cm^{-1}.

A_1		A_2		B_1		B_2	
Calc. TO/LO	Expt. TO/LO	Calc. TO	Expt. TO	Calc. TO/LO	Expt. TO	Calc. TO/LO	Expt. TO
50/50	55/55	31	–	33/33	–	63/63	**55**
58/58	**69**/–	36	**45**	76/77	**65**	76/76	69
94/94	92/–	64	**69**	101/104	92	93/93	**92**
101/101	104/–	94	102	166/173	**140**	134/135	125
166/166	**152**/–	155	**148**	263/268	257	159/159	140
181/181	218/–	250	**238**	271/281	**266**	183/183	170
260/260	**247/249**	261	**250**	281/286	**283**	265/267	**258**
280/289	–/**281**	303	**276**	310/315	**296**	283/289	**284**
293/302	**284**/–	308	**281**	387/413	**390**	295/298	**297**
311/311	297/300	387	**387**			309/310	**300**
358/358	**360/360**					355/358	**360**
385/386	**390/392**					392/394	**385**
391/405	–/–					403/413	402
53/54	–/**59**	21	–	39/39	–	68/68	68
61/62	74/74	40	–	71/72	**72**	79/80	77
105/106	102/**103**	65	74	113/115	**89**	107/104	84
111/111	110/**110**	99	97	182/207	**186**	137/137	127
198/198	**185**/–	187	**191**	258/261	**248**	181/184	**170**
208/210	–/**197**	245	**238**	273/274	–	225/225	**213**
256/257	**248/250**	255	**249**	282/289	**288**	264/264	**266**
289/292	**288/290**	300	**286**	313/313	**313**	295/295	**284**
310/313	**301/307**	310	**308**	511/544	**505**	302/308	292
317/317	**314/317**	519	**511**			315/316	**313**
398/398	**395/395**					392/393	**378**
504/507	**505/512**					523/524	**507**
507/530	–/–					526/549	**522**

geometries (e.g., the mode at 360 cm^{-1} in Cu_2CdGeS_4 is rather intense in all scattering configurations; in the case of Cu_2CdSiS_4 several modes of A_1 symmetry, even not so strong, are detected in forbidden polarizations, as marked in Fig. 6). The origin of this effect might partly be related to some positional disorder of the cation sublattice or twinning. Furthermore, due to the closeness of the excitation's laser energy ($E_{exc} = 1.92$ eV) to real electronic transitions in Cn_2CdGeS_4, the scattering processes are definitely of "resonant origin," that partially relaxes the standard scattering selection rules and moreover, due to electron-phonon coupling, typically enhances LO modes, especially the fully symmetric ones (see, e.g., Refs. [45,46] and references cited therein). But even in this case it is possible to separate most of the observed lines by symmetry by analyzing their relative intensities in the spectra.

In order to perform an assignment of the observed lines to specific eigenmodes of the lattice, we compare experimental mode frequencies with those calculated theoretically. Table II summarizes this comparison. Note that both TO and LO components of fully symmetric A_1 modes were accessed in the $x(zz)\overline{x}$ and $z(yy)\overline{z}$ scattering geometries, respectively. Most of the lines in corresponding spectra appear at the same frequency, indicating rather small LO-TO splitting. The highest frequency A_1 mode of Cu_2CdSiS_4 exhibits the largest splitting (512–505 cm^{-1}) in accordance with theory. Overall, for fully symmetric A_1-phonon excitations there seems to be a very reasonable agreement between theory and experiment

not only for the position, but also for the magnitude of LO-TO splitting.

The situation is similar for the A_2, B_1, and B_2 modes as Table II shows. So, 42(41) out of theoretically predicted 45 vibrational modes for both Cu_2CdGeS_4 (Cu_2CdSiS_4) are assigned to the specific lattice eigenmodes with good agreement between theoretical and experimental mode frequencies. Only several calculated modes are found not to have counterparts in the experimental spectra. The main reason for that is the instrumental limitation (low-frequency cutoff at about 40 cm^{-1}) so that modes with lower wave numbers could not be observed. Several modes at higher frequencies probably have their intensities below the detection limit.

It is instructive to briefly analyze displacement patterns of some vibrational modes. First of all, we focus on the high-frequency modes, which occur in the ranges of 505–522 cm^{-1} for Cu_2CdSiS_4 and 385–402 cm^{-1} in the case of Cu_2CdGeS_4; six modes in both compounds are of the following symmetries: $2A_1 + A_2 + B_1 + 2B_2$. In the case of Cu_2CdGeS_4 sulfur is by far the lightest atom among all the constituents and thus is expected to contribute primarily to those high-frequency modes. As shown in the right panel of Fig. 7 where two out of the six modes in the frequency range of interest are
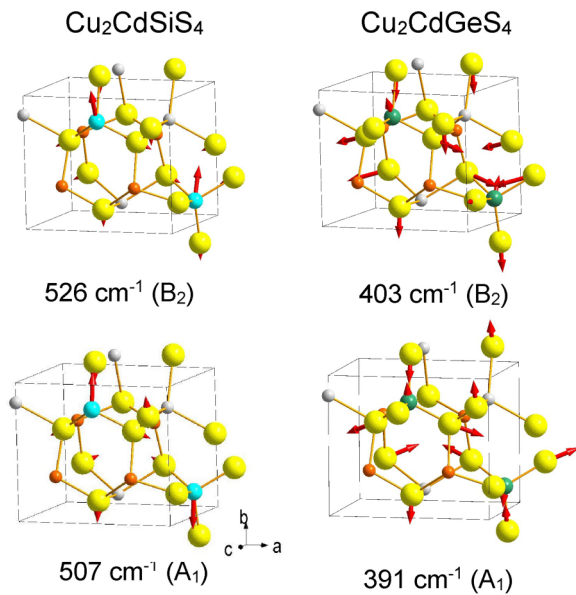
FIG. 7. (Color online) DFT-calculated ion displacements for two high-frequency vibrational modes of Cu_2CdSiS_4 (left panel) and Cu_2CdGeS_4 (right panel). Mode frequencies and symmetries are shown below each picture.

FIG. 8. (Color online) DFT-calculated modes with the same displacement patterns for Cu_2CdSiS_4 and Cu_2CdGeS_4. The atom at the position occupied by either Si or Ge is shown in blue. Corresponding vibrational frequencies and symmetries are listed for both compounds. Top and middle frames represent the most intense (experimental) modes, whereas the lowest frame represents the mode which has the same vibrational pattern and similar frequency for two materials.

depicted, this is really the case. The A_1-symmetry mode at 391 cm^{-1} and the B_2 mode at 403 cm^{-1} both involve asymmetric deformations of GeS_4 tetrahedra. One has to note that contributions of Ge displacements are sufficiently adding to these modes.

In the case of Cu_2CdSiS_4 the situation is rather different because both S and Si now have similar small masses (approximately 32 and 28 atomic units, respectively) in comparison to other constituents. As calculations show, the high-frequency modes (A_1 at 507 cm^{-1} and B_2 at 526 cm^{-1}) in this case are primarily due to Si displacements (left panel of Fig. 7), and there is only a very small contribution from S displacements.

Furthermore, having assigned the phonon modes to specific lattice eigenmodes, we may analyze the displacement pattern for phonon modes which exhibit the highest intensity in experimental spectra and thus the highest polarizability. These are the modes at about 360 cm^{-1} for Cu_2CdGeS_4 and 395 cm^{-1} for Cu_2CdSiS_4 as is obvious from Figs. 5 and 6. According to calculations, several vibrational modes in the range of interest indeed possess virtually identical displacement patterns but have different frequencies for the two compounds. In particular, the top and middle frames of Fig. 8 show the A_1 and B_2 vibrations that are predicted to occur at 398 (358) and 392 (355) cm^{-1} for Cu_2CdSiS_4 (Cu_2CdGeS_4). These vibrations involve in-phase (A_1 mode) and out-of-phase (B_2 mode) "breathing" of two SiS_4 or GeS_4 tetrahedra within the primitive unit cell. Si(Ge) ions do not participate in these vibrational modes. Thus, the high intensity of these selected modes in experimental spectra is due to simultaneous modulation of *all* Si(Ge)-S bonds. We have to also point out that Si-related vibrations in the range of 505–522 cm^{-1} possess much weaker intensity in the experimental spectra (Fig. 6) in comparison to the S-related modes due to their lower polarizability.
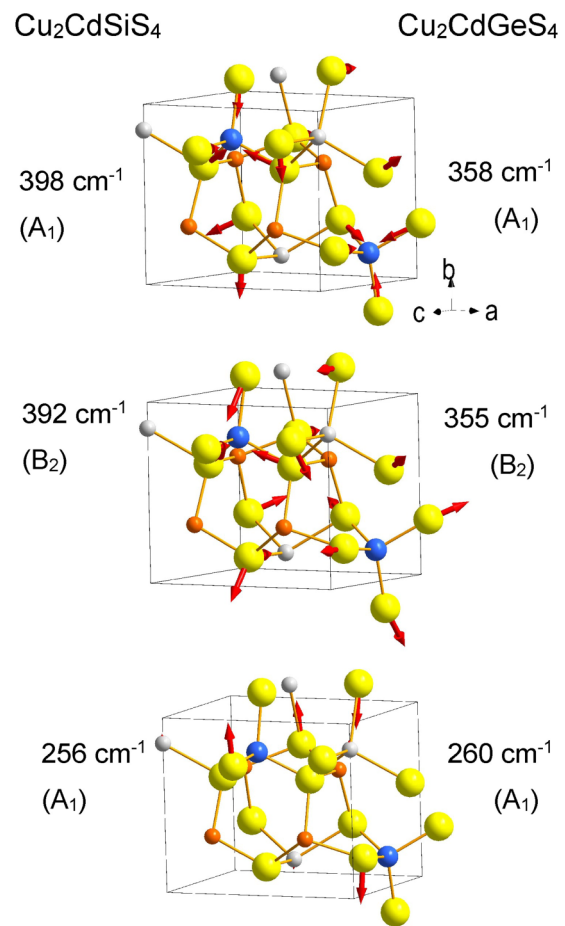
The mode in the lowest panel of Fig. 8 is an example of a vibration that has an identical displacement pattern for two materials and simultaneously a very similar frequency: 256 and 260 cm^{-1} for Cu_2CdSiS_4 and Cu_2CdGeS_4, respectively. This mode is related to the modulation of Cd-S bonds. Notably, the mode frequency of this vibration is very close to the one well known for the bulk CdS semiconductor [41] $\omega_0 = (2\omega_{TO} + \omega_{LO})/3 \approx 260$ cm^{-1}. This signals that in both Cu_2CdSiS_4 and Cu_2CdGeS_4 the CdS_4 tetrahedra are basically unperturbed with respect to those in the binary bulk CdS crystals. As a matter of fact the average Cd-S bond length, according to the DFT-calculated relaxed structure of these materials, is equal to 2.560 and 2.554 Å for Cu_2CdSiS_4 and Cu_2CdGeS_4, respectively, which only slightly exceeds the one in the bulk hexagonal or cubic CdS crystals where it is equal to 2.528 Å [41].

It is interesting in this respect to check the behavior of the vibrational modes away from the Brillouin-zone center. In Fig. 9 the calculated phonon dispersion is shown for
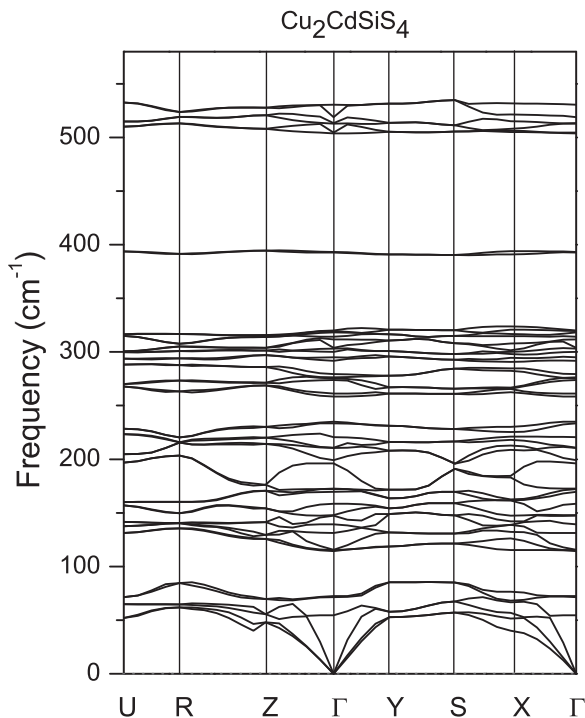
FIG. 9. DFT-calculated phonon dispersion relations across the Brillouin zone of orthorhombic Cu_2CdSiS_4.

Cu_2CdSiS_4. Obviously, the vibrational modes in the frequency range above 350 cm^{-1}, which are well separated in frequency from the other modes and, as we mentioned, are exclusively due to SiS$_4$ displacements, exhibit only marginal dispersion on the wave vector. This clearly signals that, like in a "molecular crystal," there is only very weak interaction of this structural unit with neighboring units. Vibrations at lower frequencies, especially those below 230 cm^{-1}, are much more complex, and

the majority of them involve several ions. Their frequencies, as seen from Fig. 9, vary across the Brillouin zone.

IV. CONCLUSIONS

To summarize, we have experimentally studied the spectral dependence of the dielectric function of orthorhombic (wurtz-stannite) Cu_2CdGeS_4 and Cu_2CdSiS_4 crystals by ellipsometry and analyzed it via comparison with *ab initio* calculations. The DFT-calculated spectral dependencies of real and imaginary dielectric constants reproduce reasonably well the main features in the experimental spectra. Polarized Raman-scattering measurements were performed. All experimental phonon peaks are assigned to the specific lattice eigenmodes of the wurtz-stannite structure. Good agreement between theoretical and experimental mode frequencies was established. Analysis of the calculated mode displacement patterns allowed us to unambiguously identify the strongest lines in the spectra as being due to the breathing of GeS$_4$ and SiS$_4$ octahedra.

We found that, in accordance with the group-theoretical analysis, the Raman spectrum of the wurtz-stannite phase exhibits many more peaks in comparison with stannite and kesterite and could efficiently be used as a structural characterization tool. The differences in the experimental Raman spectra of Cu_2CdGeS_4 and Cu_2CdSiS_4 are well correlated with the effect of exchanging Si and Ge predicted by calculations.

[1] S. Siebentritt and S. Schorr, Prog. Photovoltaics **20**, 512 (2012).

[2] A. Walsh, S. Chen, S.-H. Wei, and X.-G. Gong, Adv. Energy Mater. **2**, 400 (2012).

[3] I. Tsuji, Y. Shimodaira, H. Kato, H. Kobayashi, and A. Kudo, Chem. Mater. **22**, 1402 (2010).

[4] M. Ibáñez, R. Zamani, W. Li, A. Shavel, J. Arbiol, J. R. Morante, and A. Cabot, Cryst. Growth Des. **12**, 1085 (2012).

[5] X. Lin, J. Kavalakkatt, K. Kornhuber, D. Abou-Ras, S. Schorr, M. C. Lux-Steiner, and A. Ennaoui, RSC Adv. **2**, 9894 (2012).

[6] S. Chen, A. Walsh, Y. Luo, J.-H. Yang, X. G. Gong, and S.-H. Wei, Phys. Rev. B **82**, 195203 (2010).

[7] X. Fontané, V. Izquierdo-Rosa, E. Saucedo, E. Schorr, V. O. Yukhymchuk, M. Ya. Valakh, A. Pérez-Rodríguez, and J. R. Morante, J. Alloys Compd. **539**, 190 (2012).

[8] S. Levcenco, D. O. Dumcenco, Y. P. Wang, J. D. Wu, Y. S. Huang, E. Arushanov, V. Tezlevan, and K. K. Tiong, Opt. Mater. **34**, 1072 (2012).

[9] M. Leon, S. Levcenko, R. Serna, G. Gurieva, A. Nateprov, J. M. Merino, E. J. Friedrich, U. Fillat, S. Schorr, and E. Arushanov, J. Appl. Phys. **108**, 093502 (2010).

[10] O. V. Parasyuk, L. V. Piskach, Y. E. Romanyuk, I. D. Olekseyuk, V. I. Zaremba, and V. I. Pekhnyo, J. Alloys Compd. **397**, 85 (2005).

[11] Y. Zhang, X. Sun, P. Zhang, X. Yuan, F. Huang, and W. Zhang, J. Appl. Phys. **111**, 063709 (2012).

[12] Q. Shu, J.-H. Yang, S. Chen, B. Huang, H. Xiang, X.-G. Gong, and S.-H. Wei, Phys. Rev. B **87**, 115208 (2013).

[13] S. Nakamura, T. Maeda, and T. Wada, Jpn. J. Appl. Phys. **49**, 121203 (2010).

[14] N. B. Mortazavi Amiri and A. Postnikov, Phys. Rev. B **82**, 205204 (2010).

[15] F. Luckert, D. I. Hamilton, M. V. Yakushev, N. S. Beattie, G. Zoppi, M. Moynihan, I. Forbes, A. V. Karotki, A. V. Mudryi, M. Grossberg, J. Krustok, and R. W. Martin, Appl. Phys. Lett. **99**, 062104 (2011).

[16] M. Guc, A. P. Litvinchuk, S. Levcenko, V. Izquierdo-Roca, X. Fontané, M. Ya. Valakh, E. Arushanov, and A. Pérez-Rodríguez, Phys. Rev. B **89**, 205205 (2014).

[17] L. V. Piskach, O. V. Parasyuk, and Ya. E. Romanyuk, J. Alloys Compd. **299**, 227 (2000).

[18] G. Ye. Davydyuk, O. V. Parasyuk, Ya. E. Romanyuk, S. A. Semenyuk, V. I. Zaremba, L. V. Piskach, J. J. Koziol, and V. O. Halka, J. Alloys Compd. **339**, 40 (2002).

[19] L. D. Gulay, Y. E. Romanyuk, and O. V. Parasyuk, J. Alloys Compd. **347**, 193 (2002).

[20] G. E. Davidyuk, O. V. Parasyuk, S. A. Semenyuk, and Ya. E. Romanyuk, Inorg. Mater. **39**, 919 (2003).

[21] O. V. Parasyuk, Ya. E. Romanyuk, and I. D. Olekseyuk, J. Cryst. Growth **275**, e159 (2005).

[22] V. V. Filonenko, B. D. Nechiporuk, N. E. Novoselitskii, V. A. Yuchimchuk, and Y. F. Lavorik, Inorg. Mater. **27**, 83 (1991).

[23] M. G. Brik, I. V. Kityk, O. V. Parasyuk, and G. L. Myronchuk, J. Phys.: Condens. Matter **25**, 505802 (2013).

[24] M. Himmrich and H. Haeuseler, Spectrochim. Acta, Part A **47**, 933 (1991).

[25] M. Kruszynska, H. Borchert, J. Parisi, and J. Kolny-Olesiak, J. Am. Chem. Soc. **132**, 15976 (2010).

[26] V. Dzhagan, A. P. Litvinchuk, M. Ya. Valakh, M. M. Kruszynska, J. Kolny-Olesiak, C. Himcinschi, and D. R. T. Zahn, Phys. Status Solidi A **211**, 195 (2014).

[27] G. Chaouis and A. Niggli, Acta Crystallogr., Sect. B: Struct. Crystallogr. Cryst. Chem. **28**, 1626 (1972).

[28] E. Parthé, *Crystal Chemistry of Tetrahedral Structures* (Gordon & Breach, New York, 1964).

[29] F. Haidu, M. Fronk, O. D. Gordan, C. Scarlat, G. Salvan, and D. R. T. Zahn, Phys. Rev. B **84**, 195203 (2011).

[30] J. P. Perdew, K. Burke, and M. Ernzerhof, Phys. Rev. Lett. **77**, 3865 (1996).

[31] A. D. Becke, Phys. Rev. A **38**, 3098 (1988).

[32] S. J. Clark, M. D. Segall, C. J. Pickard, P. J. Hasnip, M. J. Probert, K. Z. Refson, and M. C. Payne, Z. Kristallogr. **220**, 567 (2005).

[33] B. Himmetoglu, A. Floris, S. Gironcoli, and M. Cococcioni, Int. J. Quantum Chem. **114**, 14 (2014).

[34] H. J. Monkhorst and J. D. Pack, Phys. Rev. B **13**, 5188 (1976).

[35] K. Refson, P. R. Tulip, and S. J. Clark, Phys. Rev. B **73**, 155114 (2006).

[36] J. P. Perdew and M. Levy, Phys. Rev. Lett. **51**, 1884 (1983).

[37] L. J. Sham and M. Schlüter, Phys. Rev. Lett. **51**, 1888 (1983).

[38] K. A. Johnson and N. W. Ashcroft, Phys. Rev. B **58**, 15548 (1998).

[39] C. Lee, W. Yang, and R. G. Parr, Phys. Rev. B **37**, 785 (1988).

[40] H. Xiao, J. Tahir-Kheli, and W. A. Goddard II, J. Phys. Chem. Lett. **2**, 212 (2011).

[41] P. Yu and M. Cardona, *Fundamentals of Semiconductors* (Springer, Heidelberg, 2010).

[42] D. Dumcenco and Y.-S. Huang, Opt. Mater. **35**, 419 (2013).

[43] X. Fontané, L. Calvo-Barrio, V. Izquierdo-Roca, E. Saucedo, A. Pérez-Rodríguez, J. R. Morante, D. M. Berg, P. J. Dale, and S. Siebentritt, Appl. Phys. Lett. **98**, 181905 (2011).

[44] R. Loudon, Adv. Phys. **13**, 423 (1964).

[45] *Light Scattering in Solids II*, edited by M. Cardona and G. Güntherodt (Springer, Berlin, 1982).

[46] M. V. Abrashev, A. P. Litvinchuk, C. Thomsen, and V. N. Popov, Phys. Rev. B **55**, R8638 (1997).